AIP | Journal of Applied Physics

Analysis of the radiative lifetime of Pr3+ d-f emission

Aleksander Zych, Matthijs de Lange, Celso de Mello Donegá, and Andries Meijerink

Citation: J. Appl. Phys. **112**, 013536 (2012); doi: 10.1063/1.4731735
View online: http://dx.doi.org/10.1063/1.4731735
View Table of Contents: http://jap.aip.org/resource/1/JAPIAU/v112/i1
Published by the American Institute of Physics.

Analysis of the radiative lifetime of Pr^{3+} *d-f* emission

Aleksander Zych,[a] Matthijs de Lange, Celso de Mello Donegá, and Andries Meijerink
CMI, Debye Institute for NanoMaterials Science, Utrecht University, 3508TA Utrecht, The Netherlands

(Received 5 December 2011; accepted 1 June 2012; published online 13 July 2012)

The radiative lifetime of excited states is governed by Fermi's Golden Rule. For many applications, the radiative decay rate is an important parameter. For example, for scintillators materials in PET scanners, a short response time is crucial and it has been realized that the *d-f* emission of Pr^{3+} is faster than for the widely applied *d-f* emission from Ce^{3+}. In this paper, the radiative decay rate of *d-f* emission from Pr^{3+} is systematically investigated in a wide variety of host lattices, including scintillators materials. The variation in the decay rate is analyzed based on Fermi's Golden Rule. The trend observed is best described using a full cavity model to correct for local-field effects and a λ^3 factor to account for the energy of the transition. Still, there is a considerable scatter of the experimental data around the best fit to these data. The variation is explained by uncertainties in the refractive indices and a variation in the transition dipole moment of the *d-f* transition for Pr^{3+}. Based on the results, the shortest radiative lifetime that can be achieved for Pr^{3+} *d-f* emission is predicted to be ~6 ns. © *2012 American Institute of Physics*. [http://dx.doi.org/10.1063/1.4731735]

I. INTRODUCTION

Inorganic scintillator materials with a short response time are widely investigated for application in the field of medical imaging, especially for use in the positron emission tomography (PET).[1–6] The coincident detection of two γ-rays emitted during a positron annihilation event depends strongly on the sharpness of the emission spikes generated by the absorption of γ photon by the scintillator. A faster response time improves the image resolution. Emission in scintillators materials originates from activator ions, which show luminescence after energy transfer from the host lattice to the activator. Fast emission is achieved for a fully allowed electronic transition. The present generation of PET-scanners mostly applies Ce^{3+}-doped scintillators materials. The fully allowed (parity and spin allowed) transition on the Ce^{3+} ions between the excited *5d* state and the *4f* ground state results in lifetimes between 20 and 70 ns. The energy of the emitting 5d state is influenced by the covalency of the material as well as the crystal-field splitting. Ce^{3+} emission can occur in a broad spectral range (350-600 nm). As a consequence, the emission lifetime varies widely from ~20 ns for UV emission to ~70 ns for orange emission, as predicted by Fermi's Golden Rule.[1,2] Since for PET a shorter-lived emission will improve the timing resolution of the system, Pr^{3+} *d-f* emission in inorganic host lattices is a promising alternative for Ce^{3+} *d-f* emission. The *d-f* emission of Pr^{3+} is about 2–3 times faster than *d-f* emission of Ce^{3+} because this emission is at ~12 240 cm^{-1} higher energy for Pr^{3+} than for Ce^{3+} in the same host.[7] As a result, research on scintillator materials with efficient Pr^{3+} *d-f* emission has attracted much attention in the recent years. There is however no quantitative analysis of the trend in the emission lifetimes. It is the aim of this paper to provide such an analysis and compare the results with earlier work on the *d-f* emission lifetimes for of Eu^{2+} and Ce^{3+}.[1,2] Careful experiments were conducted to accurately determine the radiative lifetime and wavelength of the *d-f* emission from Pr^{3+} in phosphates, borates, silicates, aluminates, fluorides, and oxychlorides. A clear general trend is observed: the radiative lifetime increases from 7.6 ns to 23 ns as the Pr^{3+} *d-f* emission shifts from 230 nm to 320 nm. A careful quantitative analysis and comparison with Fermi's Golden Rule is hampered by a large scatter in the data due to uncertainties in the refractive indices, different models for local-field correction and a variation in the transition dipole moment. It will be discussed that these uncertainties are similar as in previous studies on the decay times of the *d-f* emission from Eu^{2+} and Ce^{3+}.

II. EXPERIMENTAL

A. Measurements

The luminescence spectra and luminescence decay curves have been measured using synchrotron radiation at SUPERLUMI station (DESY, Hamburg). A detailed description of the set-up can be found elsewhere.[8] The synchrotron spectra were measured in three time windows (integrated, fast and slow) making it possible to distinguish between fast and slow emissions. The fast time window extended from 2 to 14 ns, while the slow time window was set between about 100 and 200 ns after the ps synchrotron excitation pulse. Excitation spectra were corrected for variation of the intensity as a function of wavelength using the excitation spectrum of sodium salicylate as a reference. The emission spectra were not corrected for detector response. Luminescence decay curves were recorded using time correlated photon counting with a time resolution of ~200 ps, mainly limited by the response time of the MCP detector (Hamamatsu R6358p). Time to amplitude conversion (TAC) and pulse height

[a]Author to whom correspondence should be addressed. Electronic mail: alek_zych@yahoo.com or a.k.zych@uu.nl.

analysis (PHA) has been used to measure luminescence decay curves. The sample temperature could be varied between ~8 K and 320 K in a cold finger helium cryostat. Luminescence lifetimes and luminescence spectra were recorded at different temperatures. For the analysis of the radiative decay times, the low temperature values under excitation in the *fd* band were used, since non-radiative processes are suppressed at low temperatures and excitation in the *fd* band of Pr^{3+} prevents possible delayed emission related to energy transfer from the host lattice.

B. Choice of investigated systems

The measurements of the radiative decay time of emission have been conducted in a variety of systems, including fluorides and chlorides, phosphates, borates, silicates, and aluminates. The synthesis of the materials was done according to conventional solid state synthesis techniques. The phase purity was checked by x-ray powder diffraction. The materials have different crystal structures and a variation of refractive index values between 1.5 and 2.0 at the wavelengths for the Pr^{3+} *d-f* emission (225-315 nm). The values of the refractive indices were taken from the literature or have been estimated using literature data for similar compounds.[9–19] The host lattices investigated have relatively large bandgaps, which are required to position the lowest energy *fd* state of Pr^{3+} within the forbidden gap of the materials. If the *fd* levels are in or close to the edge of the conduction band, (temperature induced) quenching of the luminescence occurs due to photoionization processes. The doping concentrations for Pr^{3+} were low (0.05%–0.2%) in order to prevent cross-relaxation between Pr^{3+} neighbors, which shortens the lifetime. The list of materials investigated is summarized in Table I. Note that for many of the materials, extensive literature exists on the *d-f* luminescence properties (spectra and decay time) of Pr^{3+}. Nevertheless, it turned out to be very difficult to extract reliable and consistent data on the radiative lifetime of the Pr^{3+} *d-f* emission in many of the materials investigated. Discrepancies in the reported values can result from high Pr-concentrations (quenching by cross-relaxation), elevated temperatures (temperature quenching), host lattice/x-ray excitation (delayed feeding), or other unknown issues related to luminescence decay time measurements. It is for this reason that low-doped systems were synthesized and investigated using the same experimental set-ups, aimed at carefully determining the radiative lifetime of the Pr^{3+} *d-f* emission.

III. THEORETICAL BACKGROUND

In a two-level system, the spontaneous emission rate (Γ_R) for an electronic transition depends on the emission wavelength, the refractive index n of the host material, and the transition dipole moment of the transition, as described by Fermi's Golden Rule for an electric dipole transitions[1,21,22,29,30]

$$\Gamma_R = 64\pi^4/3h \times \chi \times v^3 \times |\mu_{if}|^2. \quad (1)$$

In this equation, χ is the local-field correction factor, which is function of n, v is the energy of the transition (in cm^{-1}), and μ_{if} is the transition dipole moment for the electric dipole transition between the initial and final state. An alternative expression that is often encountered in the literature is

$$\Gamma_R = 1.5\,10^{-4} \times f \times \chi/\lambda^2, \quad (2)$$

where f is the oscillator strength of the transition and λ is the wavelength of the transition (in nm). For *f-d* transitions, the expression

$$\Gamma_R = 4.34\,10^{-4} \times [|\langle 5d|r|4f\rangle_{eff}|^2] \times \chi \times v^3 \quad (3)$$

has been derived from Fermi's Golden Rule. Here, $|\langle 5d|r|4f\rangle_{eff}|$ is the radial integral for the *f-d* transition. Based on Eq. (2), sometimes it is argued that there should be a quadratic rather than a cubic relation between the radiative lifetime and the emission wavelength.[1,31] However, one

TABLE I. Radiative decay times for the Pr^{3+} *d-f* luminescence in a variety of host lattices. λ is the emission wavelength in nm, τ_{exp} is the experimental emission lifetime in ns, n is the refractive index of the material at the emission wavelength, χ_{full} is the local-field correction value for the full cavity model, and χ_{empty} is the local-field correction value for the empty cavity model. The last two columns give emission wavelength and radiative decay time, respectively, for the Ce^{3+} *d-f* luminescence for comparison, with a reference to the literature.

Host lattice	λ (nm)	τ_{exp}(ns)	n	χ_{full}	χ_{empty}	Ce^{3+} λ (nm)	Ce^{3+} τ_{exp}(ns)
$LiYF_4$	225	18.1	1.53[9]	3.2	2.3	306 (Ref. 20)	28.61[20]
YPO_4	242	11.8	1.75 (Refs. 10 and 11)	5	2.9	345 (Ref. 22)	23[22]
$LaPO_4$	228	13.4	1.8 (Ref. 11)	5.5	3	365 (Ref. 23)	19[23]
$LuPO_4$	245	15.4	1.72 (Refs. 10, 11, and 13)	4.7	2.8	360 (Ref. 1)	25[1]
$ScBO_3$	265	15.7	1.9 (Ref. 12)	6.6	3.3	375 (Ref. 24)	23[24]
$LuBO_3$	257	16.1	1.9 (Refs. 12 and 13)	6.6	3.3	370 (Ref. 24)	26[24]
YBO_3	260	14.5	1.9 (Ref. 13)	6.6	3.3	383 (Ref. 25)	
$LaBO_3$	245	12.7	1.85 (Ref. 14)	6	3.2	352 (Ref. 25)	
$YAlO_3$ (YAP)	247	7.5	2.03 (Ref. 15)	8.5	3.6	362 (Refs. 22)	17.1[22]
$Y_3Al_5O_{12}$ (YAG)	315	23.3	1.9 (Ref. 16)	6.6	3.3	535 (Ref. 22)	65[22]
$Lu_3Al_5O_{12}$ (LuAG)	308	18	1.87 (Refs. 13 and 16)	6.3	3.2	497 (Ref. 26)	54[26]
Y_2SiO_5 (YSO)	271	20.4	1.79 (Refs. 11 and 17)	5.4	3	420 (Ref. 27)	40[27]
Lu_2SiO_5 (LSO)	270	20	1.82 (Refs. 11 and 18)	5.7	3.1	420 (Ref. 22)	40[22]
LaOCl	260	12	2.1 (Ref. 19)	9.6	3.8	420 (Ref. 28)	17[28]

should realize that the oscillator strength is linearly proportional to ν,[30] which results in an overall increase of Γ_R with ν^3, consistent with Eqs. (1) and (3).

To describe the influence of the local-field on the transition probability, many models have been developed to correct for the interaction of the two-level system with the surrounding dielectric medium.[21,22,29,32] Mostly, two models are considered, the empty (or real) cavity model for which

$$\chi = n \times [3n^2/(2n^2+1)]^2 \quad (4)$$

and the full (or virtual) cavity model, which is based on the Lorentz local-field and gives

$$\chi = n \times [(n^2+2)/3]^2. \quad (5)$$

The difference between the two models is in the refractive index of the cavity where the luminescent ion or molecule resides. For the full cavity model, n is assumed to be the same as for the surrounding host, whereas for in the empty cavity model, it is different.[21,32] Many different models have been developed in addition to these two models, including microscopic models based on the interaction between the emitter and local dipoles,[33,34] but experimental verification of the various models is challenging.[35]

It is not known which model is valid for lanthanide luminescence. The real cavity model has been suggested in the literature for intraconfigurational *f-f* emissions of Eu^{3+},[21] while the full cavity model has been proposed for the interconfigurational *d-f* luminescence of Ce^{3+}.[1,22,31] The most recent study suggest that in both cases (*f-f* and *d-f* transitions of lanthanides), the full cavity model is appropriate, since the lanthanide ions have very low polarizability and do not disturb the host material around themselves when being doped into the host matrix, thus they do not create a real cavity.[36] Neither the hand waving arguments used to justify the use of one model over the other nor the experimental evidence for either model have been convincing.[1,21,22,31] Due to the uncertainties, both local-field correction models will be discussed and compared. From the expressions for the local-field correction, one can see that the dependence on the refractive index is much stronger in case of the full (virtual) cavity model. The dependence of the local-field correction factor on the refractive index is illustrated in Fig. 1.

In the past experimental and theoretical work has been done on the relation between the radiative lifetime and emission wavelength for the *d-f* emission from Ce^{3+} and Eu^{2+}.[1,21,22,31,37] In case of the investigations for Eu^{2+} and Ce^{3+}, a single *d-f* emission wavelength is used for λ. This is a good approximation, since the emission band is confined in narrow spectral region due to transition from the *5d* state to a single $4f^7(^8S_{7/2})$ ground state of Eu^{2+} or two $4f^1$-states separated by only 2000 cm^{-1}, the $^2F_{5/2}$ and $^2F_{7/2}$ states of Ce^{3+}. For Pr^{3+} *d-f* emission is observed over a wider spectral range. The strongest transitions are to the $^3H_4$ ground state, but typically four emission bands can be observed, spanning in the range of about 10 000 cm^{-1}, the energy difference between the $^3H_4$ ground state and the $^1G_4$ excited $4f^2$ state. Typical emission spectra of Pr^{3+} *d-f* emission will be shown in Sec. IV. A more appropriate procedure would involve taking a weighted average of wavelengths and wavelength dependent refractive indices of the material to calculate Γ_R. In view of the larger uncertainties in the various other parameters, we have chosen to use a single emission wavelength and refractive index for the strongest and highest energy emission band in the analysis of the wavelength dependence of the decay time.

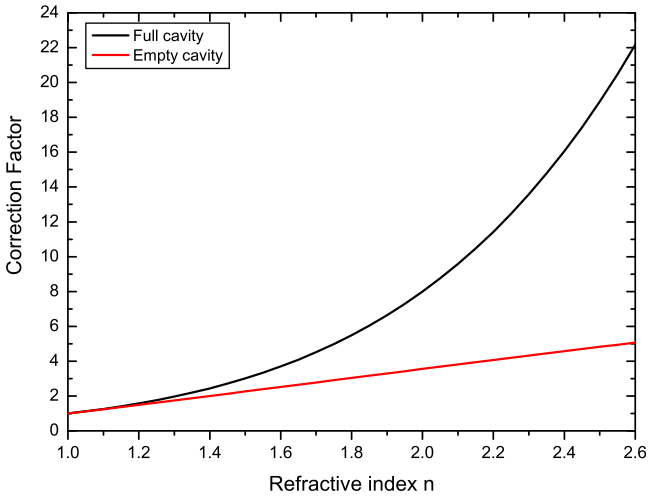

FIG. 1. Dependence of the value of the local-field correction factor on the refractive index of the material, for the full (black curve) and empty (red curve) cavity models.

IV. RESULTS AND DISCUSSION

In this section, the luminescence properties and luminescence decay times for Pr^{3+} in a variety of host lattices will be shown and compared, where possible, to results reported in the literature. For some host lattices, extensive data exist in the literature. The large variation in luminescence lifetimes reported warrants a brief overview of our results on low doped systems and a comparison and discussion with reported literature data to provide a background to the data collected in Table I.

A. Aluminates

Aluminates are among the most widely studied materials when it comes to *d-f* luminescence of lanthanides. For Ce^{3+}, Eu^{2+}, and also Pr^{3+}, the *d-f* emission has been studied in variety of aluminates and resulted in application of Eu^{2+} doped aluminates in fluorescent tubes and afterglow materials[38,39] and Ce-doped aluminates in scintillators crystals[27,40] and white light emitting diodes (LEDs).[41,42] The luminescence of Pr^{3+} in aluminates has been especially studied in the garnets $Y_3Al_5O_{12}$ (YAG) and $Lu_3Al_5O_{12}$ (LuAG). In the garnet structure, there is one crystallographic site for the large lanthanide ion, which has dodecahedral symmetry. LuAG:Pr has great potential as a fast scintillator material. In Fig. 2, the excitation and emission spectra and the luminescence decay curve are shown for LuAG doped with 0.1% Pr^{3+}. The luminescence spectra are consistent with previous reports: *f-d* excitation bands are observed at 240 nm and 285 nm, while below 190 nm, strong host lattice (HL)

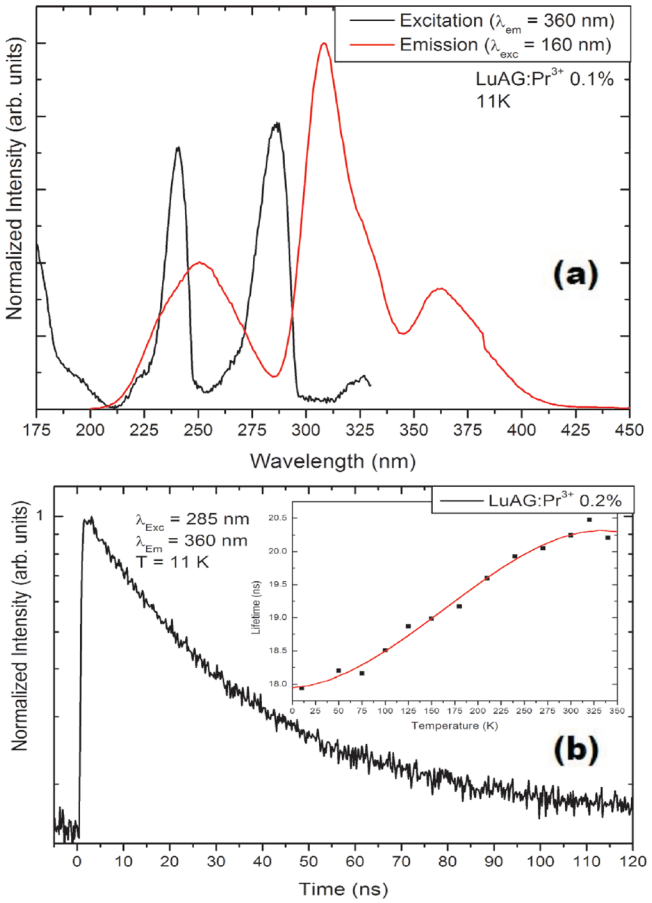

FIG. 2. (a) Excitation (black curve) and emission (red curve) spectra of LuAG:Pr^{3+} at 11 K. (b) Luminescence decay curve for Pr^{3+} *d-f* emission in LuAG under direct *fd* excitation at 11 K. The inset shows the temperature dependence of the Pr^{3+} *d-f* emission lifetime.

absorption is observed, indicating that energy transfer from the HL to the *fd* excited state of Pr^{3+} is efficient. Especially in low-doped systems, where the direct absorption into the *fd* band is weak due to the low activator concentration, a high relative intensity of the host lattice absorption band in the excitation spectrum of the *d-f* emission is a good measure for the energy transfer efficiency to the *fd* state of Pr^{3+}. Emission bands at 308 nm and 364 nm correspond to transitions from the lowest *fd* state to the ($^3H_4$, $^3H_5$) and ($^3H_6$, ^3F_J (J = 2-4)) states within the $4f^2$ configuration. The luminescence decay curve at 4 K is single exponential with an 18.2 ns decay time. At room temperature, a longer decay time is measured, 21.3 ns. The increase of the decay time temperature is peculiar and is plotted in the inset in Fig. 2. Probably, thermal occupation of a higher energy *fd* state which has a lower decay rate is responsible for the lengthening of the decay time. The presently found values for the luminescence decay times are consistent with values in the literature, although there is some variation in the values reported. Room temperature decay times between 19 and 25 ns have been reported.[43–45] A careful temperature dependent study on low Pr-doped (0.25%) LuAG crystals reports an 18 ns lifetime at 4 K increasing to 21 ns at RT, consistent with the present findings.[43–45]

For YAG:Pr^{3+} 0.1%, the excitation and emission band for the lowest energy $^3H_4 \rightarrow$ *fd* transition has shifted to slightly longer wavelengths, 315 nm in emission and 288 nm in excitation. The redshift of the lowest *fd* state of Pr^{3+} in YAG with respect to LuAG has also been observed for *d-f* emission from Ce^{3+} in LuAG and YAG and is unexpected. For the smaller Lu^{3+}-cation site, compared with Y^{3+}, a larger crystal-field splitting is expected to shift the lowest *fd* to lower energies in LuAG. Calculations have been done to explain this unexpected shift but have not been able to fully clarify the observations.[46] The luminescence lifetime of the *d-f* emission for Pr^{3+} in YAG is 21.5 ns and decreases to 13.5 ns at RT. The drop is explained by temperature quenching, which causes the intensity and decay time of the *d-f* emission of Pr^{3+} in YAG to decrease between 150 and 350 K. In the literature decay times at 4 K between 18 and 22 ns have been reported while for RT similar values (13–14 ns) have been found.[47,48]

The perovskite aluminate $YAlO_3$ (yttrium aluminate perovskite or YAP) is not easy to synthesize. Often additional crystalline phases, especially the garnet phase, are formed during the synthesis. In the perovskite structure, the lanthanide ion is in a cubic twelve coordination. In Fig. 3, the luminescence spectra and luminescence decay curves for the *d-f* emission of Pr^{3+} in YAP are shown. The sample investigated did contain YAG:Pr^{3+} as a second phase, but the higher energy *d-f* emission from Pr^{3+} in YAP could be

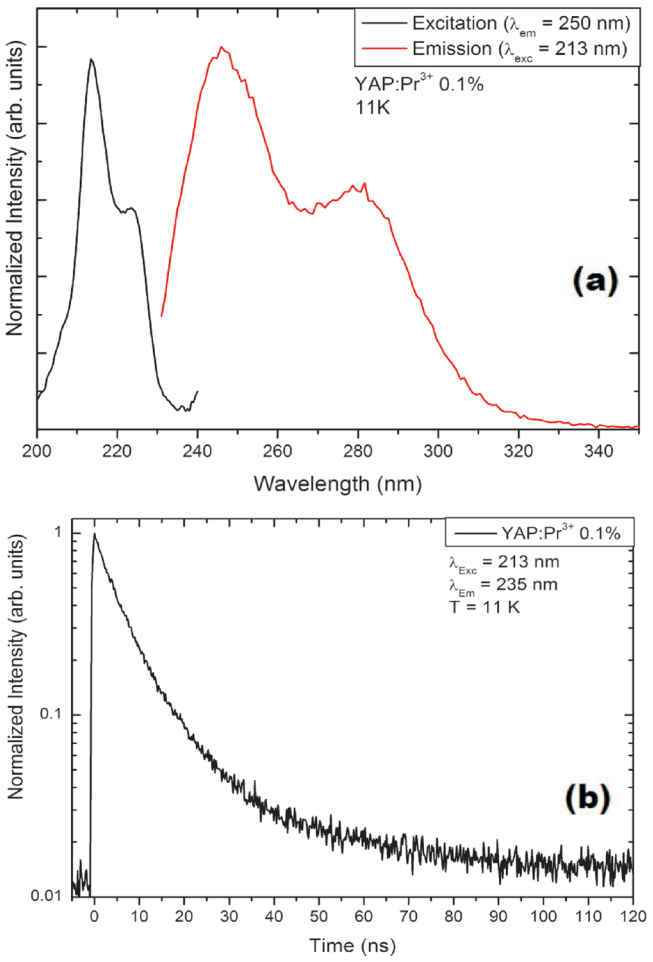

FIG. 3. (a) Excitation (black curve) and emission (red curve) spectra of YAP:Pr^{3+} at 11 K. (b) Luminescence decay curve for Pr^{3+} *d-f* emission in YAP under direct *fd* excitation at 11 K.

selectively monitored. The excitation spectra show a double band between 210 and 230 nm for the transition to the lowest energy *fd* state. In the emission spectrum, the highest energy band is observed at 247 nm (transition to the $^3H_4$, $^3H_5$ state) and the 280 nm emission band is assigned to the transition to the $^3H_6$, $^3F_2$ states at ~5000 cm^{-1} higher energy. The emission spectrum is similar to the spectrum reported in the literature for YAP:Pr^{3+} for a low doped (0.05%) crystal.[49] At higher doping concentrations, the relative intensity of the 247 nm band was observed to decrease due to reabsorption. The luminescence decay curve recorded for the *d-f* emission under *fd* excitation is depicted in Fig. 3(b). The decay curve is close to single exponential with a decay time of 7.5 ns. This short decay time is consistent with values reported in the literature. In Ref. 49, decay curves of the Pr^{3+} *d-f* emission were reported for pulsed x-ray excitation. The decay curves showed a multi-exponential decay, with a short time component of 7–10 ns related to the radiative decay of the *d-f* emission and a longer time component of 100–200 ns, probably due to slower feeding processes related to trapping and de-trapping processes after host lattice excitation. The presently observed decay time of 7.5 ns is consistent with the short radiative lifetimes reported in Ref. 49.

B. Orthoborates

Orthoborates MBO_3 (M = Sc, Lu, Y, La) are well-known host lattices for luminescence studies and have been doped with a variety of trivalent lanthanide ions.[50–52] The crystal structure varies: for the smaller cations (Sc and Lu), the orthoborates have the calcite structures with a six-coordination for the lanthanide ion. YBO_3 has a vaterite related structure with two crystallographic sites for the trivalent ion (6 or 6 + 6 coordination), and in $LaBO_3$ with the aragonite structure, the trivalent ion is in 9-coordination.[53] In Figs. 4–7, the luminescence spectra and luminescence decay curves are shown for the Pr-doped orthoborates. The emission spectra reveal a four-band structure corresponding to transitions from the lowest *fd* state to the $^3H_4$, $^3H_5$, $^3H_6/^3F_2$, and $^3F_3/^3F_4$ states. For the Sc, Lu, and Y, the four bands are well-resolved due to the small band widths as a result of small Stokes shifts. For $LaBO_3$, the bands are broadened. The positions of the highest energy emission bands are 265 nm (Sc), 257 nm (Lu), 260 nm (Y), and 245 nm (La). The general trend of a shift to higher energies for larger cation sites is explained by a reduction in crystal-field splitting. The slight anomaly for the Lu and Y (the larger Y ion host shows a lower energy Pr^{3+} *d-f* emission) can be related to the change in crystal structure. The excitation spectra of the *d-f* emission reveal a structured lowest energy *fd* band between 210 and 250 nm for Sc, Y, and Lu and a host lattice absorption band with an onset at 180 nm (Sc) or 165 nm (Lu, Y). For $LaBO_3$, the crystal-field splitting for the lower site symmetry results in multiple *fd* excitation bands (230 nm and 200 nm). The third band with an onset at 190 may be a third crystal-field component or be related to host lattice absorption. The luminescence decay curves of the *d-f* emission shows a single exponential decay with decay times of 15.7 ns (Sc), 16.1 ns (Lu), 14.5 ns (Y), and 12.7 ns (La). The decay

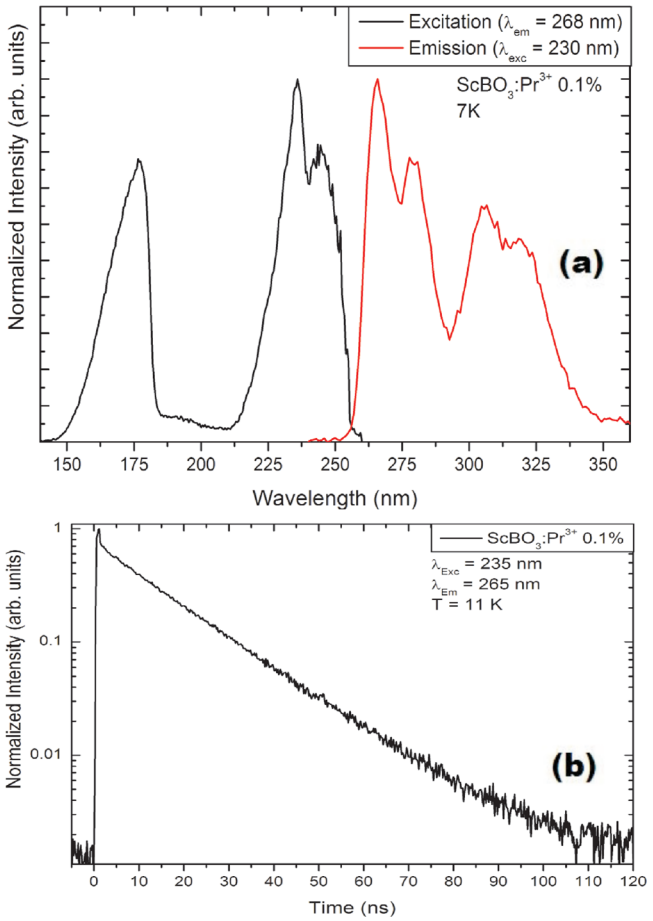

FIG. 4. (a) Excitation (black curve) and emission (red curve) spectra of $ScBO_3$:Pr^{3+} at 7 K. (b) Luminescence decay curve for Pr^{3+} *d-f* emission in $ScBO_3$ under direct *fd* excitation at 11 K.

decreases with increasing energy of the emitting *fd* state. Note that there is an irregularity in some of the decay curves (La and Lu) after 10 ns. This is an instrumental artifact. The decay times were determined from single exponential fits starting after the artifact. The luminescence spectra for Pr^{3+} in Sc, Y, and La orthoborate have been reported before.[50,54] The emission spectra are consistent with previous results. The presently reported excitation spectra show that the position of the lowest energy *fd* excitation band is at slightly shorter wavelength than reported in Ref. 50, which can be explained by instrumental limitations due to the use of a Xe-lamp in Ref. 50. The luminescence decay time reported for the *d-f* emission in $Lu_{0.8}Sc_{0.2}BO_3$ is shorter (11.9 ns) than the presently reported values (~16 ns for $LuBO_3$ and $ScBO_3$). Both the higher Pr concentration (0.5% in Ref. 54) and higher temperature (RT in Ref. 54) can be responsible for the shorter lifetimes due to concentration quenching and/or temperature quenching.

C. Orthophosphates

The orthophosphates have been model systems in the study *fd* spectra of lanthanide ions. The small Stokes shift for the *d-f* luminescence in YPO_4 allows for the observation of fine structure (zero-phonon lines and vibronic side bands) in the *f-d* excitation and the *d-f* emission spectra.[55–58]

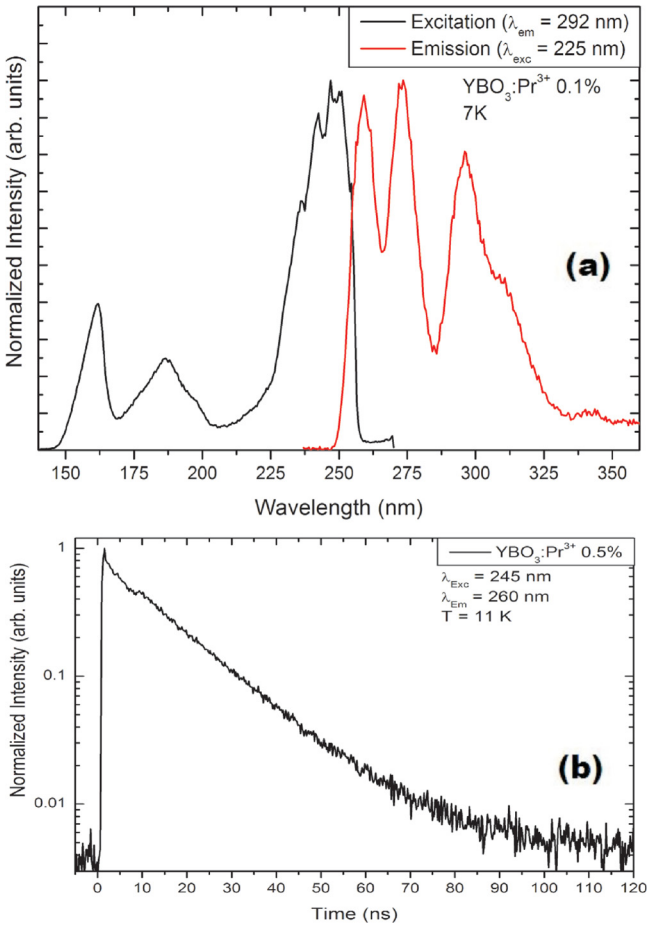

FIG. 5. (a) Excitation (black curve) and emission (red curve) spectra of $YBO_3:Pr^{3+}$ at 7 K. (b) Luminescence decay curve for Pr^{3+} *d-f* emission in YBO_3 under direct *fd* excitation at 11 K.

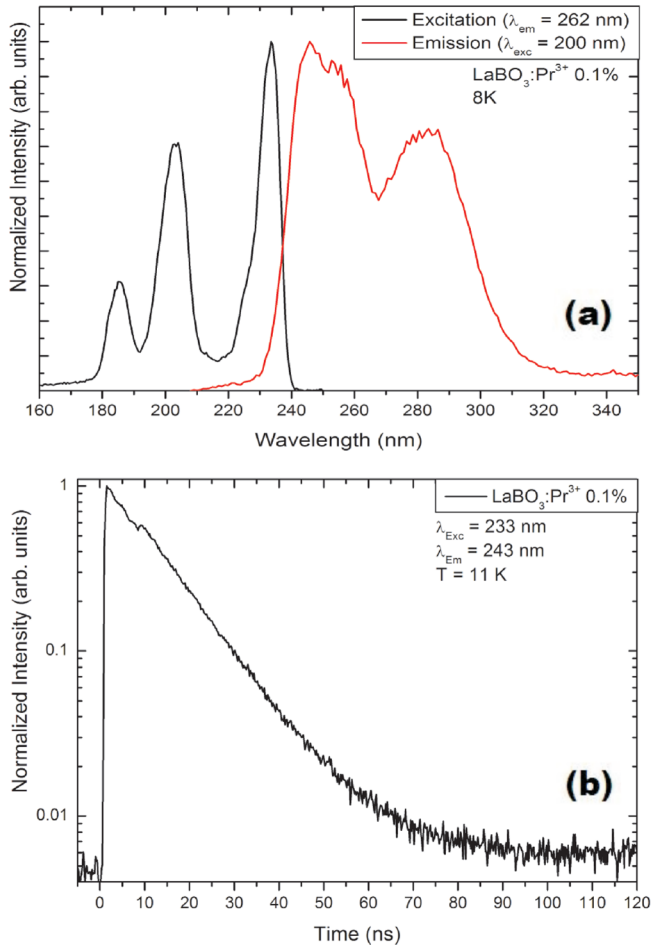

FIG. 6. (a) Excitation (black curve) and emission (red curve) spectra of $LaBO_3:Pr^{3+}$ at 8 K. (b) Luminescence decay curve for Pr^{3+} *d-f* emission in $LaBO_3$ under direct *fd* excitation at 11 K.

Systematic studies of the *fd* spectra for the lanthanides in YPO_4 have aided in the development of theoretical models explaining the energy level structure in $4f^{n-1}5d$ excited states. In Fig. 8, the excitation and emission spectra of Pr^{3+} in YPO_4 are shown. The emission spectrum shows two emission bands with maxima at 242 and 260 nm, with a shoulder on the short wavelength side of the 242 nm band. The large spectral width is due to the poor spectral resolution of the emission monochromator. The luminescence spectra for $YPO_4:Pr^{3+}$ reported in the literature show narrow bands with vibrational structure at low temperatures with a weaker band around 233 nm and stronger bands peaking at 242 and 260 nm, in agreement with the presently reported spectra.[56,58,59] The excitation spectrum shows fine structure for the lowest energy *fd* band around 225 nm. At higher energies, *fd* bands are observed around 180 and 150 nm. The luminescence decay of the *d-f* emission (shown in Fig. 8(b)) is single exponential with decay time of 11.8 ns. In the literature, longer lifetimes have been reported (17 ns),[60] which may be related to the time resolution of the pulsed xenon lamp used in Ref. 60. For $LuPO_4$ doped with Pr^{3+}, the luminescence spectra are similar and red-shifted by a few nm (Fig. 9). The luminescence decay time is longer: 15.4 ns. For Pr^{3+} in $LaPO_4$, the lowest energy *fd* level has shifted to higher energies due to a smaller crystal-field splitting. In Fig. 10, the luminescence spectra are shown. The excitation and emission bands corresponding to transitions involving the lowest energy *fd* state are around 205 and 228 nm, respectively. The luminescence decay curve for the *d-f* emission is shown in Fig. 10(b). The decay is single exponential with a decay time of 13.4 ns. Previous work on $LaPO_4:Pr^{3+}$ has shown interesting Pr^{3+} luminescence in $LaPO_4$, including emission from the $^1S_0$ level in competition with non-radiative decay to the lowest *fd* state.[61] The luminescence spectra are in agreement with those in the literature.[61,62] As far as we are aware, no lifetime has been reported for the *d-f* luminescence for Pr^{3+} in $LaPO_4$.

D. Oxyorthosilicates

The oxyorthosilicates Y_2SiO_5 (YSO) and Lu_2SiO_5 (LSO) host lattices doped with lanthanides are used in a variety of applications, including cathode ray tube (CRT) phosphors, scintillator, and optical data storage.[27] LSO and the high temperature modification of YSO have the same (monoclinic) crystal structure in which there are two crystallographic sites for the rare earth ions with 6 and 7 coordination by oxygen. Luminescence from Pr^{3+} in both YSO and LSO has been studied extensively.[59,63–66] In Fig. 11, the luminescence spectra and decay curve are shown for YSO doped with 0.1% of Pr^{3+}. In the excitation spectrum, *fd* excitation

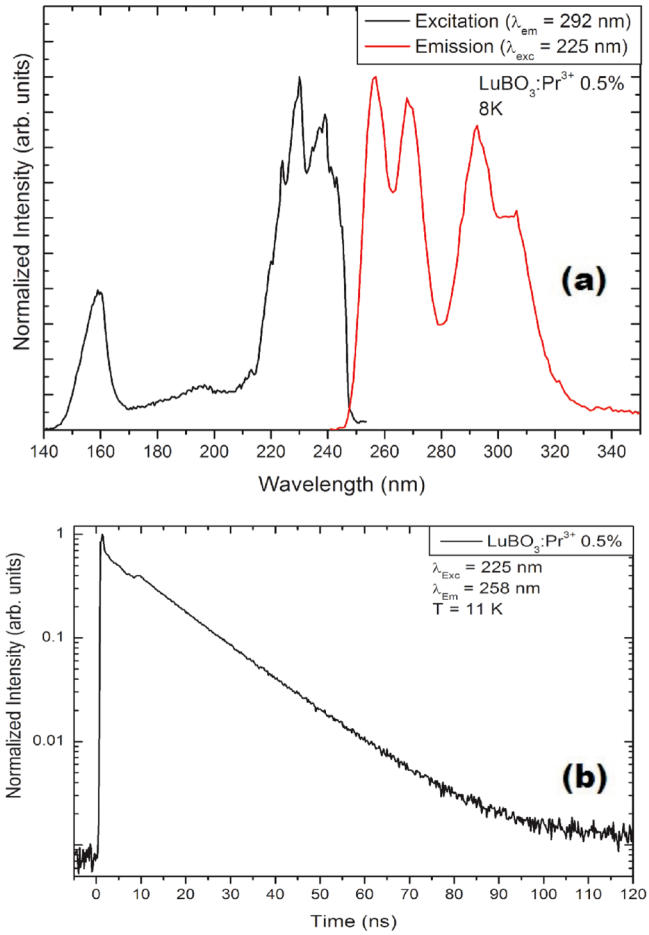

FIG. 7. (a) Excitation (black curve) and emission (red curve) spectra of $LuBO_3$:Pr^{3+} at 8 K. (b) Luminescence decay curve for Pr^{3+} *d-f* emission in $LuBO_3$ under direct *fd* excitation at 11 K.

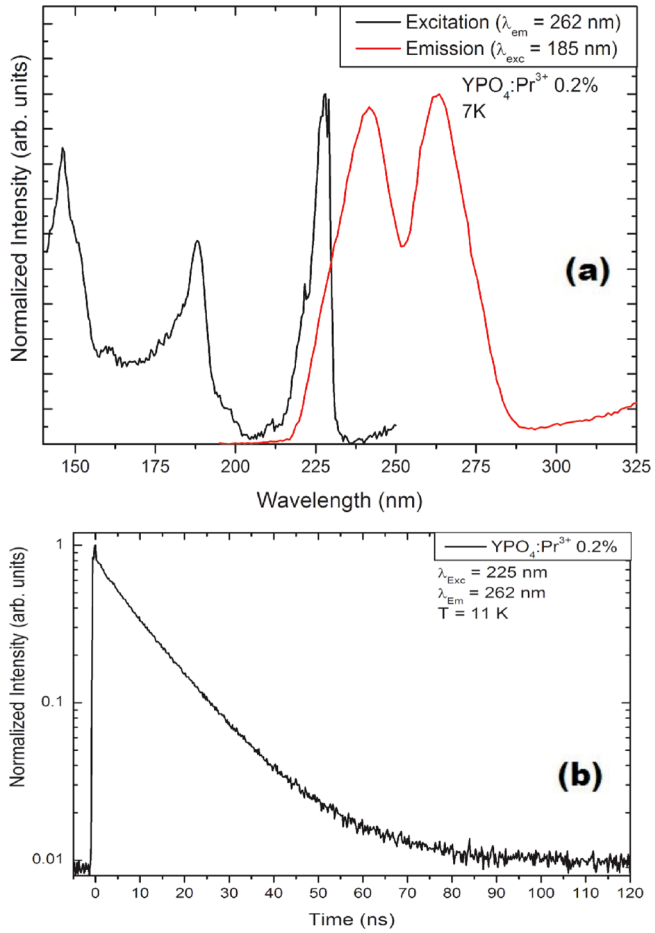

FIG. 8. (a) Excitation (black curve) and emission (red curve) spectra of YPO_4:Pr^{3+} at 7 K. (b) Luminescence decay curve for Pr^{3+} *d-f* emission in YPO_4 under direct *fd* excitation at 11 K.

bands are observed around 248 and 220 nm. Below 200 nm, the host lattice absorption starts. The highest energy emission band has a maximum at 271 nm and is assigned to the transition to the $^3H_{4,5}$ ground state. For Pr^{3+} in LSO, the luminescence spectra are very similar. In Fig. 11(b), the luminescence decay curve of the *d-f* emission from Pr^{3+} is shown. The decay is single exponential with a decay time of 20.4 ns. The low temperature decay time of the *d-f* emission is also the same for Pr^{3+} in LSO and YSO, for Pr^{3+} in LSO, a decay time of 20 ns is found. For YSO, the room temperature decay is very similar to the room temperature decay time, 19.5 ns. For Pr^{3+} in LSO, temperature quenching reduces the decay time. The presently reported spectra are in good agreement with spectra reported in the literature.[59,63–66] The luminescence decay times reported in the literature vary. For Pr^{3+} in LSO low temperature decay times of 25 ns (Ref. 63) or 7 and 26 ns (Ref. 64) have been reported. At room temperature, the decay is shortened by thermal quenching to 6 ns.[63] For YSO the decay time for the *d-f* emission from Pr^{3+} has been reported to be 30 ns (Ref. 66) and 17 ns.[65] The latter value is close to the presently observed 19.5 ns decay time.

E. Other host lattices

In addition to the classes of host lattices discussed above, the *d-f* luminescence for Pr^{3+} has been investigated two other compounds: $LiYF_4$ and LaOCl. $LiYF_4$ is a model system for studies in lanthanide spectroscopy, both for providing insight in intraconfigurational $4f^n$-$4f^n$ and interconfigurational $4f^n$-$4f^{n-1}5d$ transitions. In Fig. 12, the excitation and emission spectra for Pr^{3+} in $LiYF_4$ are shown. The emission spectrum shows bands around 225 and 248 nm while the excitation spectrum consists of three bands between 140 and 220 nm. The emission bands can be assigned to transitions from lowest energy *fd* state to the $^3H_4$ and $^3H_5$ levels (225 nm) and the $^3H_6$ and $^3F_{3,4}$ levels (248 nm). The large spectral width is due to the poor resolution of the emission monochromator. Higher resolution emission spectra have been reported in which sharp zero-phonon lines and vibronic lines are observed and the transitions to the $^3H_4$, $^3H_5$, and $^3H_6$ levels are spectrally well-resolved.[58] Careful spectroscopic investigations have also revealed fine structure in the excitation spectra, which cannot be observed in Fig. 12 due to the low spectral resolution of the experimental set-up. For the present study, the vibronic features are not important. The spectra are in agreement with those reported in the literature. The luminescence decay curve shows a purely single exponential decay with a characteristic decay time of 18.1 ns. In the literature, different decay times have been reported for the *d-f* emission of Pr^{3+} in $LiYF_4$, sometimes significantly

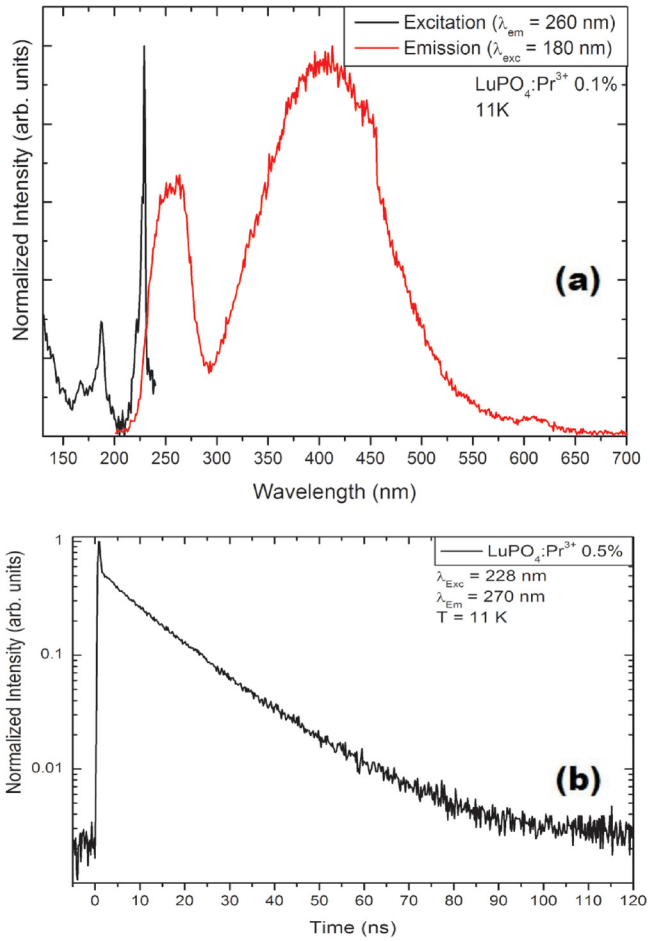

FIG. 9. (a) Excitation (black curve) and emission (red curve) spectra of $LuPO_4:Pr^{3+}$ measured at 11 K. (b) Luminescence decay curve for Pr^{3+} *d-f* emission in $LuPO_4$ under direct *fd* excitation at 11 K.

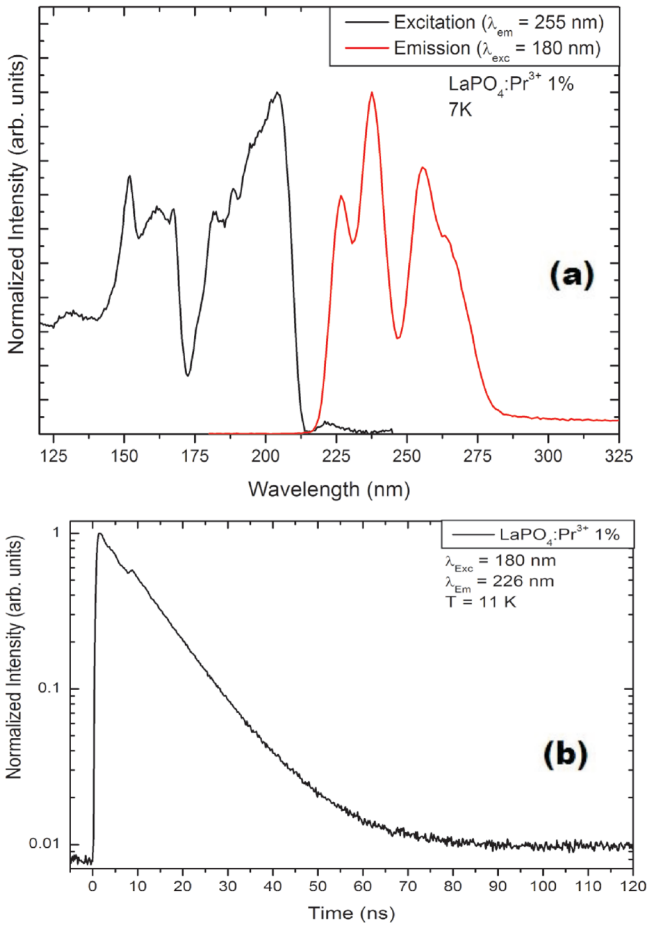

FIG. 10. (a) Excitation (black curve) and emission (red curve) spectra of $LaPO_4:Pr^{3+}$ at 7 K. (b) Luminescence decay curve for Pr^{3+} *d-f* emission in $LaPO_4$ under direct *fd* excitation at 11 K.

different from the presently determined value of 18.1 ns (e.g., 26 ns in Ref. 60) or quite similar (e.g., 19 ns in Ref. 67). As discussed above, based on the careful experiments with a fast response (~200 ps), detection system on a low-doped system where lengthening of the decay time by reabsorption or shortening by concentration quenching is prevented, the presently reported decay times are considered to be reliable.

For Pr^{3+} in LaOCl, extensive literature exists on the splitting of the $4f^2$ levels, but research on *fd* transitions is limited. In Fig. 13(a), the excitation and emission spectra are shown. The excitation onset is just below 240 nm and *fd* excitation bands are observed at 225 nm (with a shoulder on the short wavelength side) and 200 nm. The absence of host lattice absorption bands in the excitation spectrum of the *d-f* emission shows that energy transfer from the host lattice to the *fd* excited state is inefficient. Broad *d-f* emission bands are observed between 240 and 300 nm. The luminescence decay curves of the emission are close to single exponential with a decay time of ~12 ns. In the literature, no *d-f* emission from Pr^{3+} has been reported as far as we are aware. vacuum ultraviolet (VUV) excitation spectra of *f-f* emissions in Ref. 68 show three *fd* excitation bands between 240 and 180 nm, similar to the presently reported excitation spectrum.

V. GENERAL DISCUSSION

The radiative lifetimes of the *d-f* emission for Pr^{3+} in a variety of host lattices vary from 7.5 ns to 23.3 ns. In Table I, the lifetimes and information on the emission wavelength of the highest energy emission band and the refractive index are collected. In Fig. 14, the lifetimes are plotted as a function of emission wavelength. Clearly, there is a trend showing that longer lifetimes are observed for longer emission wavelengths. The scatter in the data is however large. In order to be able to better compare the measured lifetimes with the theoretical models, the data have been re-plotted as $\chi \times \tau$ (the radiative lifetimes from Table I multiplied by χ to correct for the local-field). Figure 15 shows the results using the correction factor for the empty cavity model, while the results after correction for the full cavity model are shown in Fig. 16. The theoretically predicted increase in radiative lifetime for longer emission wavelength is more clearly observed after correcting for local-field effects. Still, there is a significant scatter of the data points. Using the correction factor predicted by the full cavity model (Fig. 16) seems to be slightly better (less scatter in the data points) than for the empty cavity model (Fig. 15), but the difference is not sufficient to decide that either of the models is the correct model. In order to compare the results with theory, the wavelength

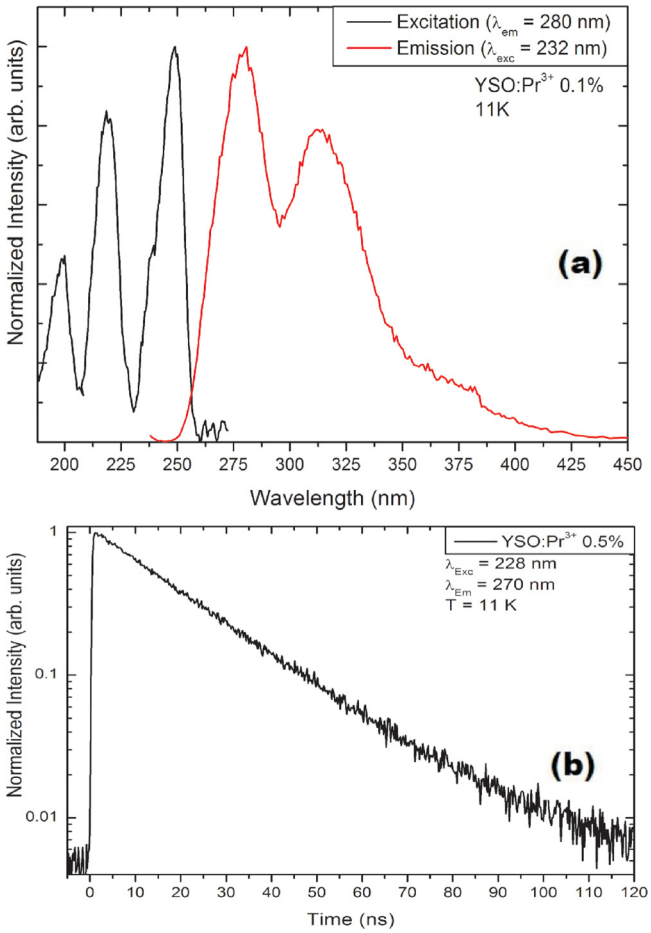

FIG. 11. (a) Excitation (black curve) and emission (red curve) spectra of YSO:Pr^{3+} at 11 K. (b) Luminescence decay curve for Pr^{3+} *d-f* emission in YSO under direct *fd* excitation measured at 11 K.

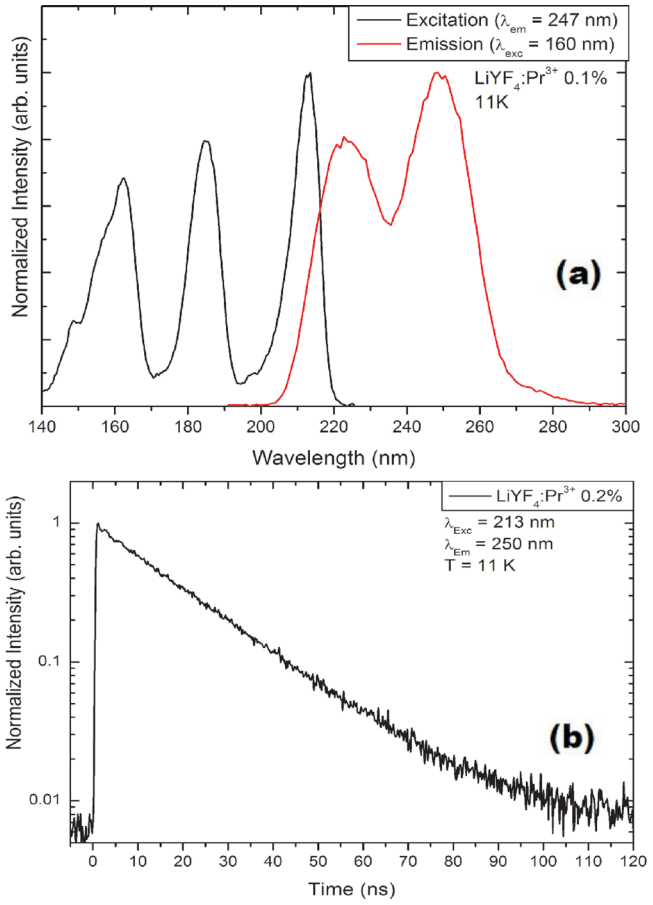

FIG. 12. (a) Excitation (black curve) and emission (red curve) spectra of $LiYF_4$:Pr^{3+} at 11 K. (b) Luminescence decay curve for Pr^{3+} *d-f* emission in $LiYF_4$ under direct *fd* excitation at 11 K.

dependence of the lifetimes, after correction for the local-field, was fitted to both a squared and a cubic wavelength dependence. The blue lines in Figs. 15 and 16 represent the fits to a λ^2 and the red lines to a λ^3 dependence. The agreement is better for the λ^3 dependence, as expected (see theory). For the λ^2 fits, the data point on short wavelength side (below 260 nm) are below the line for the best fit, while for longer wavelength, the data points are above the line. Clearly, the wavelength dependence of the radiative lifetime is steeper than a λ^2 dependence. The data points for the λ^3 fit are scattered around the line and data points are found above and below the line over the full wavelength range, indicating that the theoretically predicted λ^3 dependence gives a better agreement with experiment. From the scatter in the data around the λ^3 line, it is also clear that Eq. (3) cannot be used for an accurate calculation of the radiative lifetime, once the emission wavelength of the *d-f* emission and the refractive index of the host are known. Below, we will discuss the origin for this observation. The quality of the fit for the data corrected using the full cavity model is slightly better than for the data corrected using the empty cavity model, favoring the use of χ for the full cavity model (Eq. (5)) for *d-f* emission, in line with the results in Ref. 21. Again, it should be noted that the large scatter of the data does not allow for definite conclusions.

It is important to understand the factors that contribute to the deviation between experiment and theory. We see two main contributions. The first is the uncertainty in the values for the refractive index. It is difficult to find accurate numbers for the refractive index for many of the crystalline hosts in the UV part of the spectrum. The data collected in Table I are the most reliable estimates for n that could be obtained. Often n had to be estimated from values given for similar host lattices or values for n in the visible range. Because of the strong variation of χ with n, a more accurate determination of the refractive index will improve the reliability of the experimental data points. This will also help to provide support for which of the models for χ is correct.

A second source for the deviation of the experimental data from a smooth λ^3 dependence is the variation in the transition dipole moment $\langle 5d|r|4f\rangle_{\text{eff}}$. For a perfect λ^3 dependence, there should be no change in transition dipole moment. In first approximation, this assumption is justified. The *f-d* transition is a fully allowed electric dipole transition. For forbidden transitions, the local environment has a strong influence on the radiative lifetime, since the partial lifting of selection rules through, e.g., spin-orbit coupling or admixture of opposite parity states depends on the nature and symmetry of surrounding neighbors. For parity allowed transitions, there is no such influence. For a pure *d-f* transition, the transition dipole moment is constant. For the free ion, the

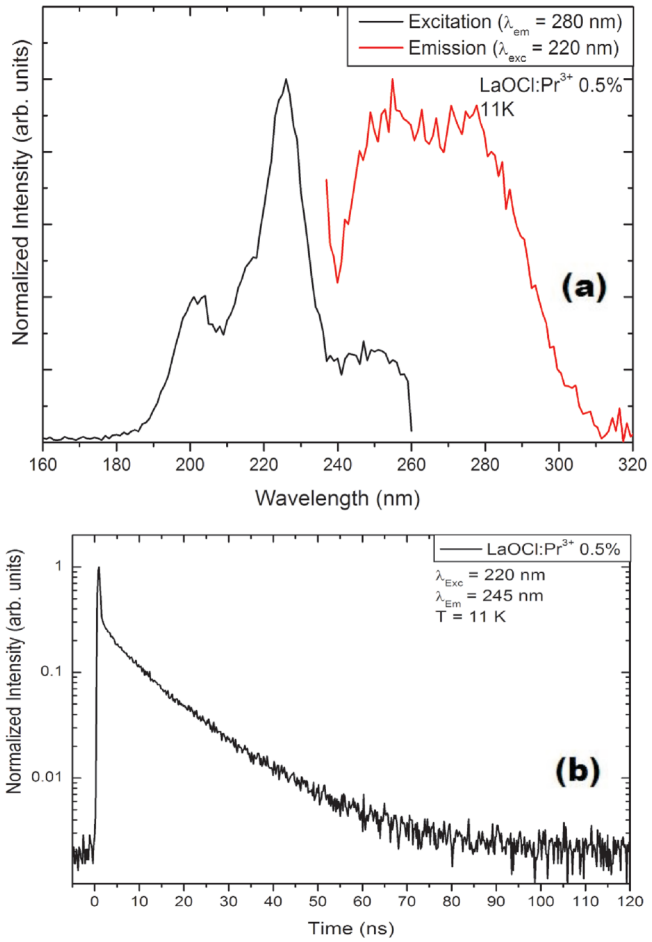

FIG. 13. (a) Excitation (black curve) and emission (red curve) spectra of LaOCl:Pr^{3+} at 11 K. (b) Luminescence decay curve for Pr^{3+} *d-f* emission in LaOCl under direct *fd* excitation at 11 K.

transition dipole moment for the *f-d* transition on Pr^{3+} has been calculated to be 0.0271.[29] However, through the nephelauxetic effect, delocalization of the *5d* orbital over the ligands can reduce the transition dipole moment below the free ion value. Differences in covalency will affect the delocalization and cause a variation in $|\langle 5d|r|4f\rangle_{\mathrm{eff}}|$. In the literature, this is recognized. In studies on the wavelength dependence of the lifetime of the *d-f* emission for Eu^{2+} [37] and Ce^{3+},[29] the transition dipole moments were calculated from the measured lifetimes, using Eq. (3) assuming a full cavity model for χ. The variation in the calculated transition dipole moments for Eu^{2+} and Ce^{3+} in Refs. 29 and 37 is large, 30%–40%, very similar to the presently observed deviation of the data points in Figs. 15 and 16 from the fitted curves representing the λ^3 dependence. Based on these observations, we can conclude that the experimentally observed wavelength dependence of the lifetime of the *d-f* emission for Ce^{3+}, Eu^{2+}, and Pr^{3+} follows Eq. (3), but there is a 30%–40% scatter to which both uncertainties in *n* and a variation in $|\langle 5d|r|4f\rangle_{\mathrm{eff}}|$ between host lattices contributed. To improve the modeling, a more accurate determination of *n* and a better insight in the variation of $|\langle 5d|r|4f\rangle_{\mathrm{eff}}|$ in different host lattices, e.g., through *ab initio* calculations of the wave functions in the *4f* ground state and $4f^{n-1}5d$ excited states[46] can contribute. In Table I, we have also included reference values of the *d-f* emission lifetime of trivalent cerium in the

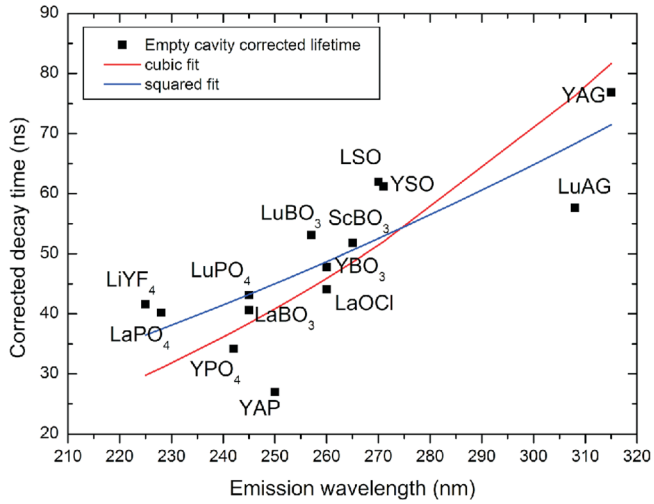

FIG. 15. Dependence of the corrected radiative lifetime on the emission wavelength of investigated systems, using the empty cavity correction.

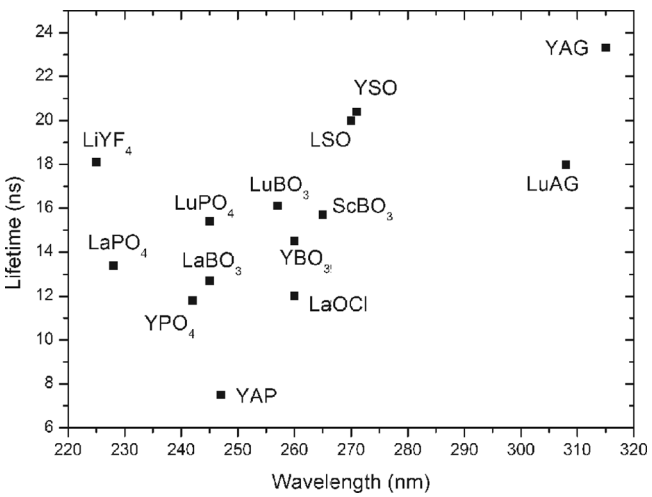

FIG. 14. Dependence of the uncorrected radiative lifetime on the emission wavelength of investigated systems.

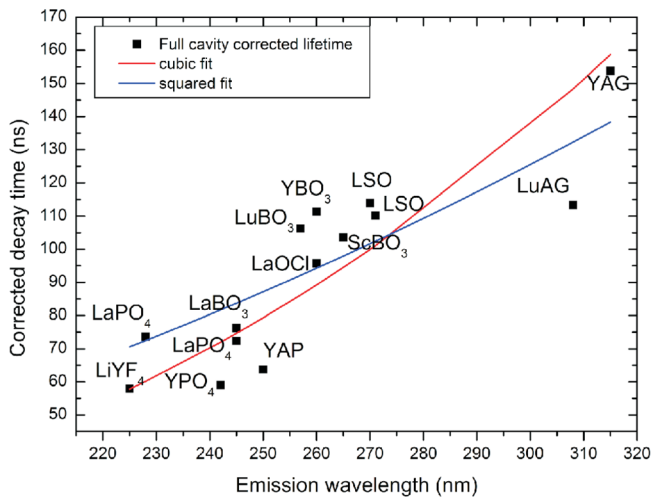

FIG. 16. Dependence of the corrected radiative lifetime on the emission wavelength of investigated systems, using the full cavity correction.

corresponding compounds. The literature data shown are mostly based low doped systems, low temperature measurement, and for excitation in the lowest *fd* level of Ce^{3+}. The trends in the *d-f* emission life times for Ce^{3+} are consistent with the observations for Pr^{3+}, but there is no perfect correlation again indicating that also variations in the transition dipole moment contribute to variation of the life time of *d-f* emission for lanthanides.

In addition to the two major factors contributing to the deviation of the data points from the fits to Eq. (3), several minor sources can be identified. In our modeling, we used a single emission wavelength for the Pr^{3+} *d-f* emission. Clearly, the emission covers a wide spectral region (wider than for Eu^{2+} and Ce^{3+}) with the most intense bands spread over about 10 000 cm^{-1}. As discussed above, it would be more correct to calculate a wavelength and intensity weighted λ^3 factor from high resolution emission spectra. This laborious procedure is however estimated to reduce the scatter in the data by less than 10%. The strongest emission bands always correspond to transitions at the highest energies and the variation in the intensity distribution for the $4f5d$-$4f^2$ emission spectra is not large (see Figs. 2–13). Even more accurate would be to also include the wavelength dependence of n in the analysis. As long as the uncertainty in the other parameters (values of n and $|\langle 5d|r|4f\rangle_{eff}|$) is so much larger, no effort was made to include these refinements. The accuracy of the measured radiative lifetimes is also important. As discussed, care was taken to determine the radiative lifetime with the highest possible accuracy by systematic research on low-doped systems at cryogenic temperatures and using sensitive and fast (sub-ns) detection schemes. The high quality and single exponential character of the decay curves give confidence that the error in the reported radiative lifetimes is small. In many cases, the lifetimes were determined for multiple combinations of *f-d* excitation and *d-f* emission wavelengths giving rise to very consistent data, with variations in the lifetimes for *d-f* emission for Pr^{3+} in a specific host lattice well below 5%. The accuracy of the experimentally determined lifetimes is clearly not a bottleneck. Note however that careful measurements are needed as values reported in the literature for lifetime of the *d-f* emission in a specific host can vary strongly due to a variety of factors (e.g., excitation over the band gap, concentration quenching, temperature quenching, and limited time resolution of the system).

The best fit of the experimentally measured radiative lifetimes has been obtained assuming a full cavity model for the local-field correction and a λ^3 dependence. The fit parameter for $|\langle 5d|r|4f\rangle_{eff}|$ for the best fit (red curve in Fig. 16) is 0.0214 nm. This value is slightly smaller than the free ion value of 0.0271. The 20% reduction can be explained by the nephelauxetic effect. Based on the present results, a reasonable estimate for the decay time of the *d-f* emission can be obtained from

$$\Gamma_R = 1/\tau = 4.34\,10^{-4} \times [|\langle 5d|r|4f\rangle_{eff}|^2] \times \chi \times \nu^3$$

with $|\langle 5d|r|4f\rangle_{eff}| = 0.0214$ and $\chi = n \times [(n^2+2)/3]^2$. To estimate the fastest decay time possible for Pr^{3+}, we need to consider that the short wavelength limit for the *d-f* emission from Pr^{3+} is about 220 nm, taking into account a small Stokes shift and the fact that the *fd* state of Pr^{3+} needs to be below the $^1S_0$ $4f^2$ level of Pr^{3+} around 212 nm.[33] The refractive index of the material at the emission wavelength should be as large as possible. An upper limit is estimated to be ~1.8 for a material in which the *d-f* emission is at high energies. Based on these considerations, the shortest radiative lifetime of the Pr^{3+} *d-f* emission at 220 nm in a material with an assumed refractive index of 1.8 is about 6 ns.

VI. CONCLUSIONS

The luminescence decay times of *d-f* emission of Pr^{3+} have been investigated in a variety of host lattices. The radiative decay times vary between 7.5 and 23 ns and show a clear correlation with wavelength: longer lifetimes are observed for longer wavelength emission. The general trend is in agreement with the Fermi's Golden Rule, but the scatter in the data is significant. The best agreement between experiment and theory is obtained for a λ^3 wavelength dependence and using the full cavity model for the local-field correction factor χ. The main contribution to deviations from the theoretical relation are the lack of reliable values for the refractive index n (needed to calculate χ) in the UV spectral region and a variation in the transition dipole moment for the *d-f* transition for Pr^{3+} in different host lattices. A more reliable determination of n may improve the accuracy, but the variation in transition dipole moment is inherent to *d-f* transitions and has also been observed for Eu^{2+} and Ce^{3+}. Since the transition dipole moment varies, a calculation of the radiative lifetime of *d-f* is not possible from the emission wavelength and refractive index. Still, radiative lifetimes can be estimated using an average value for $\langle 5d|r|4f\rangle_{eff}$ of 0.0214 nm. Using this value, the shortest lifetime that can be achieved for *d-f* emission from Pr^{3+} is estimated to be ~6 ns. This gives a lower limit for the radiative lifetime in inorganic scintillators based on luminescent ions.

ACKNOWLEDGMENTS

The authors wish to acknowledge the financial support from the EU String Project (NMP3-CT-2006-032636) as well as Dr. A. Kotlov for help during the measurements at the Superlumi beam line at HASYLAB, DESY (Hamburg).

[1]A. Lempicki and A. J. Wojtowicz, J. Lumin. **60&61**, 942–947 (1994).
[2]P. Dorenbos, *Radiation Detectors for Medical Applications*, edited by S. Tavernier *et al*. (Springer, 2006), pp. 191–207.
[3]L. Pidol, A. Kahn-Harari, B. Viana, B. Ferrand, P. Dorenbos, J. T. M. de Haas, C. W. E. van Eijk, and E. Virey, J. Phys.: Condens. Matter **15**, 2091–2102 (2003).
[4]L. Pidol, B. Viana, A. Galtayries, and P. Dorenbos, Phys. Rev. B **72**, 125110 (2005).
[5]A. Zych, A. Leferink, O. P. Reinink, K. van der Eerden, C. de Mello Donegá, and A. Meijerink, J. Alloys Compd. **509**, 4445–4451 (2011).
[6]A. Zych, C. de Mello Donegá, and A. Meijerink, Opt. Mater. **33**, 347–354 (2011).
[7]P. Dorenbos, J. Lumin. **91**, 155–176 (2000).
[8]G. Zimmerer, Nucl. Instrum. Methods A **308**, 178–186 (1991).
[9]D. E. Castleberry and A. Linz, Appl. Opt. **14**, 2056–2056 (1975).
[10]G. E. Jellison, L. A. Boatner, and C. Chen, Opt. Mater. **15**, 103–109 (2000).

[11]W. Mayr, T. Jüstel, and P. J. Schmidt, US patent 20090032772 (2 May 2009).
[12]F. Qin and R.K. Li, J. Cryst. Growth **318**, 642–644 (2010).
[13]S. Levene and C. R. Ronda, US patent 20100032578 (2 November 2010).
[14]J. Fan, Z. Lin, L. Zhang, and G. Wang, J. Phys. D: Appl. Phys. **39**, 3226–3229 (2006).
[15]S. Baccaro, A. Cecilia, M. Montecchi, T. Malatesta, F. de Notaristefani, S. Torrioli, and F. Vittori, Nucl. Instrum. Methods A **406**, 479–485 (1998).
[16]Y. Kuwano, K. Suda, N. Ishizawa, and T. Yamada, J. Cryst. Growth **260**, 159–165 (2004).
[17]C. L. Sun, J. F. Li, C. H. Hu, H. M. Jiang, and Z. K. Jiang, Eur. Phys. J. D **39**, 303–306 (2006).
[18]See http://www.apace-science.com/proteus/lso.htm for the value of the refractive index and data for other physical properties.
[19]J. Holsa and P. Porcher, J. Less-Common Met. **112**, 121–125 (1985).
[20]N. Yu. Kirikova, M. Kirm, J. C. Krupa, V. N. Makhov, E. Negodin, and J. Y. Gesland, J. Lumin. **110**, 135 (2004).
[21]D. Toptygin, J. Fluoresc. **13**, 201–219 (2003).
[22]C.-K. Duan and M. F. Reid, Curr. Appl. Phys. **6**, 348–350 (2006).
[23]J.-C. Bourcet and F. K. Fong, J. Chem. Phys. **60**, 34–39 (1974).
[24]Y. Wu, D. Ding, S. Pan, F. Yang, and G. Ren, Opt. Mater. **33**, 655 (2011).
[25]G. Blasse and A. Bril, J. Chem. Phys. **47**, 5139 (1967).
[26]M. Nikl, A. Vedda, M. Fasoli, I. Fontana, V. V. Laguta, E. Mihokova, J. Pejchal, J. Rosa, and K. Nejezchleb, Phys. Rev. B **76**, 195121 (2007).
[27]E. Zych, A. Zych, J. Zhang, and Sh. Wang, J. Alloys Compd. **451**, 286–289 (2008).
[28]Y. D. Eagleman, E. Bourret-Courchesnea, and S. E. Derenzo, *Room-temperature Scintillation Properties of Cerium-doped REOX (RE = Y,La,Gd, and Lu; X = F,Cl,Br, and I)* (Lawrence Berkeley National Laboratory, 2011).
[29]T. Chen, C.-K. Duan, and S. Xia, J. Alloys Compd. **439**, 363–366 (2007).
[30]B. Henderson and G. F. Imbusch, *Optical Spectroscopy of Inorganic Solids* (Clarendon, Oxford, 1989), pp. 315–386.
[31]E. Zych, in *Luminescence and Scintillation of Inorganic Phosphor Materials, Handbook of Luminescence, Display Materials, and Devices Vol. 2*, edited by H. S. Nalwa and L. S. Rohwer (American Scientific Publishers, 2003), pp. 251–300.
[32]K. Dolgaleva, R. W. Boyd, and P. W. Milonni, J. Opt. Soc. Am. B **24**, 516–521 (2007).
[33]I. Sokólska and S. Kück, Chem. Phys. **270**, 355–362 (2001).
[34]M. E. Crenshaw, Phys. Rev. A **78**, 053827 (2008).
[35]S. F. Wuister, C. de Mello Donegá, and A. Meijerink, J. Chem. Phys. **121**, 4311 (2004).
[36]C.-K. Duan, H. Wen, and P. A. Tanner, Phys. Rev. B **83**, 245123 (2011).
[37]S. H. M. Poort, A. Meijerink, and G. Blasse, J. Phys. Chem. Solids **58**, 1451–1456 (1997).
[38]D. Dacyl, D. Uhlich, and T. Justel, Cent. Eur. J. Chem. **7**(2), 164–167 (2009).
[39]C. Ronda, in *Emission and Excitation Mechanisms of Phosphors, Luminescence: From Theory to Applications*, edited by C. Ronda (Wiley-VCH, 2008), pp. 1–34.
[40]J. M. Ogiegło, A. Zych, K. V. Ivanovskikh, T. Justel, C. Ronda, and A. Meijerink, "Luminescence and energy transfer in $Lu_3Al_5O_{12}$ scintillators co-doped with Ce^{3+} and Tb^{3+}," Phys. Chem. (submitted).
[41]V. Bachmann, C. Ronda, and A. Meijerink, Chem. Mater. **21**, 2077–2084 (2009).
[42]K. Li and Ch. Shen, Proc. SPIE **7658**, 76583K (2010).
[43]T. Yanagida, M. Sato, K. Kamada, Y. Fujimoto, Y. Yokota, A. Yoshikawa, and V. Chani, Opt. Mater. **33**, 413 (2011).
[44]V. Babin, V. Gobrbenko, A. Krasnikov, A. Makhov, M. Nikl, S. Zazubovich, and Yu. Zorenko, Radiat. Meas. **45**, 415 (2010).
[45]Y. Shi, X. Q. Feng, Y. B. Pan, J. Zhou, Y. Huang, and Z. H. Gao, Radiat. Meas. **45**, 457 (2010).
[46]A. B. Munoz-Garcia, J. P. Pascual, Z. Barandiaran, and L. Seijo, Phys. Rev B **82**, 064114 (2010).
[47]H. Ogino, A. Yoshikawa, M. Nikl, A. Krasnikov, K. Kamada, and T. Fukuda, J. Cryst. Growth **287**, 335 (2006).
[48]J. Pejchal, M. Nikl, E. Mihokova, J. A. Mares, A. Yoshikawa, H. Ogino, K. M. Schillemat, A. Krasnikov, A. Vedda, K. Nejezchleb, and V. Mucka, J. Phys.: Appl. Phys **42**, 055117 (2009).
[49]T. Yanagida, K. Kamada, Y. Fujimoto, M. Sugiyama, Y. Furuya, A. Yamaji, Y. Yokota, and A. Yoshikawa, Nucl. Instrum. Methods Phys. Res. A **523**, 1020 (2010).
[50]G. Blasse, J. P. M. van Vliet, J. W. M. Verwey, R. Hoogendam, and M. Wiegel, J. Phys. Chem. Solids **50**, 583–585 (1989).
[51]G. Blasse and G. J. Dirken, Inorg. Chim. Acta **145**, 303–308 (1988).
[52]A. M. Srivastava, M. T. Sobieraj, S. K. Ruan, and E. Banks, Mater. Res. Bull. **21**, 1455–1463 (1986).
[53]A. Wolfert, E. W. J. L. Oomen, and G. Blasse, J. Lumin. **31**, 308 (1984).
[54]Y. Wu, D. Ding, Sh. Pan, F. Yang, and G. Ren, J. Alloys Compd. **509**, 7139–7142 (2011).
[55]R. T. Wegh, W. van Klinken, and A. Meijerink, Phys. Rev. B **64**, 045115 (2001).
[56]L. van Pieterson, M. F. Reid, R. T. Wegh, S. Soverna, and A. Meijerink, Phys. Rev. B **65**, 045113 (2002).
[57]L. van Pieterson, M. F. Reid, G. W. Burdick, and A. Meijerink, Phys. Rev. B **65**, 045114 (2002).
[58]P. S. Peijzel, P. Vergeer, A. Meijerink, M. F. Reid, L. A. Boatner, and G. W. Burdick, Phys. Rev. B **71**, 045116 (2005).
[59]M. Nikl, A. Yoshikawa, A. Vedda, and T. Fukuda, J. Cryst. Growth **292**, 416 (2006).
[60]M. Laroche, S. Girard, J. Margerie, R. Moncorge, M. Bettinelli, and E. Cavalli, J. Phys.: Condens. Matter **13**, 765 (2001).
[61]A. M. Srivastava, A. A. Setlur, H. A. Comanzo, W. W. Beers, U. Happek, and P. Schmidt, Opt. Mater. **33**, 292 (2011).
[62]E. Nakazawa and F. Shiga, Jpn. J. Appl. Phys., Part **421**, 1642 (2003).
[63]M. Nikl, H. Ogino, A. Yoshikawa, E. Mihokova, J. Pejchal, A. Beitlerova, A. Novoselov, and T. Fukuda, Chem. Phys. Lett. **410**, 218 (2005).
[64]K. Yang, M. A. Spurrier, H. Rothfuss, L. Eriksson, and C. L. Melcher, IEEE Trans. Nucl. Sci. **56**, 968 (2009).
[65]A. Novoselov, H. Ogino, A. Yoshikawa, M. Nikl, J. Pejchal, J. A. Mares, A. Beitlerova, C. D. Ambrosio, and T. Fukuda, J. Cryst. Growth **287**, 309 (2006).
[66]P. Dorenbos, M. Marsman, C. W. E. van Eijk, M. V. Korzhik, and B. I. Minkov, Radiat. Eff. Defects Solids **135**, 325 (1995).
[67]L. van Pieterson, M. F. Reid, R. T. Wegh, and A. Meijerink, J. Chem Phys. **115**, 9382 (2001).
[68]Th. Troster and W. B. Holzapfel, Phys. Rev. B **66**, 075114 (2002).